J Mol Model (2004) 10:121–129
DOI 10.1007/s00894-004-0178-9

ORIGINAL PAPER

Roy U. Rojas Wahl

Decomposition mechanism of 3-*N*-morpholinosydnonimine (SIN-1)—a density functional study on intrinsic structures and reactivities

Received: 24 April 2003 / Accepted: 28 November 2003 / Published online: 2 March 2004

Abstract Selected intrinsic aspects of the mode of action of 3-*N*-morpholinosydnonimine (**SIN-1**) and its follow-up products are investigated by means of density functional theory. Besides the well known radical-cationic Feelisch–Schoenafinger pathway, an alternative anionic route via a neutral radical is proposed and included in the study. The individual reaction pathways are followed. Most notably, the overall activation barrier for the cationic route is calculated to be 184.04 kcal mol^{-1}, while the one for the anionic route is predicted to be more favorable with 14.09 kcal mol^{-1}.

Keywords 1,2,3-Oxadiazolium-5-amidines · *N*-Nitrosohydrazines · Nitric oxide

Introduction

The chemistry, biology, pharmacology and other uses of the sydnonimine **SIN-1** have been described many times. [1, 2] Its use as an NO donor can have diverse implications that range from the rather well explored cardiovascular and cytotoxic effects [3] via stimulation of muscarinic acetylcholine receptors [4] to repair functions in neurogenesis in the brain. [5] There, more specifically, NO has been implicated with demyelination effects, [6] leading eventually to diseases such as multiple sclerosis, Parkinson's, Alzheimer's or possibly behavioral disorders such as autism. [7] Interestingly, inhibition of supraoptic oxytocin and vasopressin neurons has been reported. [8] Also, using **SIN-1**, increased permeability of the often critical blood–brain barrier has been reported. [9]

Most notably, Feelisch and Schoenafinger have developed a first good understanding of its mechanism of action, [10] as referred to in Scheme 1, where the one-electron oxidation of **SIN-1a** has been reported to be of generic nature using a variety of electron acceptors. [11]

While most theoretical and physico-chemical studies dealt with sydnones such as **SIN-1**'s clinical prodrug molsidomine, [12, 13] which has recently been associated with alleviating certain aspects of memory loss, [14] only little is known about sydnonimines and especially about the structural and reactive properties of **SIN-1** itself, as well as of any of its postulated and/or identified decomposition products depicted in Scheme 1. For **SIN-1a**, for example, noteworthy observations here concern photoactivation [15] and the fact that cyclodextrins can slow down its decomposition rate. [16]

The aim of this work is therefore to fill this gap by describing some of the intrinsic structural and reactive properties of the species shown in Scheme 1, with emphasis on two decomposition pathways: The already mentioned Feelisch–Schoenafinger mechanism and a hypothetical anionic pathway, which might be of importance when using higher pHs such as in [2].

Approach, theory and methods

Computational pathology is an integral part of the approach taken in this work. The studies follow the flow outlined in Scheme 1, starting with **SIN-1**, ending with **SIN-1c**. Each structure shown represents the conformer of the molecule that is believed to result from its predecessor in the reaction sequence. Wherever lower energy conformers exist, they are mentioned as well, and conversion barriers are discussed.

In an effort to maximize quality and minimize cost, the density functional theory (DFT) with non-local corrections to the local electron density according to the perturbative Becke [17]–Perdew [18] (pBP) theory, with a DN** [19] numerical basis set was employed. Recently, this level of theory has been shown to provide results very similar in quality to those of the computationally much more demanding Quadratic Configuration Interaction and

Dedicated to Professor Dr. Dieter Schinzer, and to the memory of Professor Sir Derek Barton, FRS.

R. U. Rojas Wahl (✉)
Initiative for Molecular Studies in Autism (IMSA),
516 North Street, Teaneck, NJ 07666, USA
e-mail: rrojaswahl@msn.com
Tel.: +1-201-836-1714

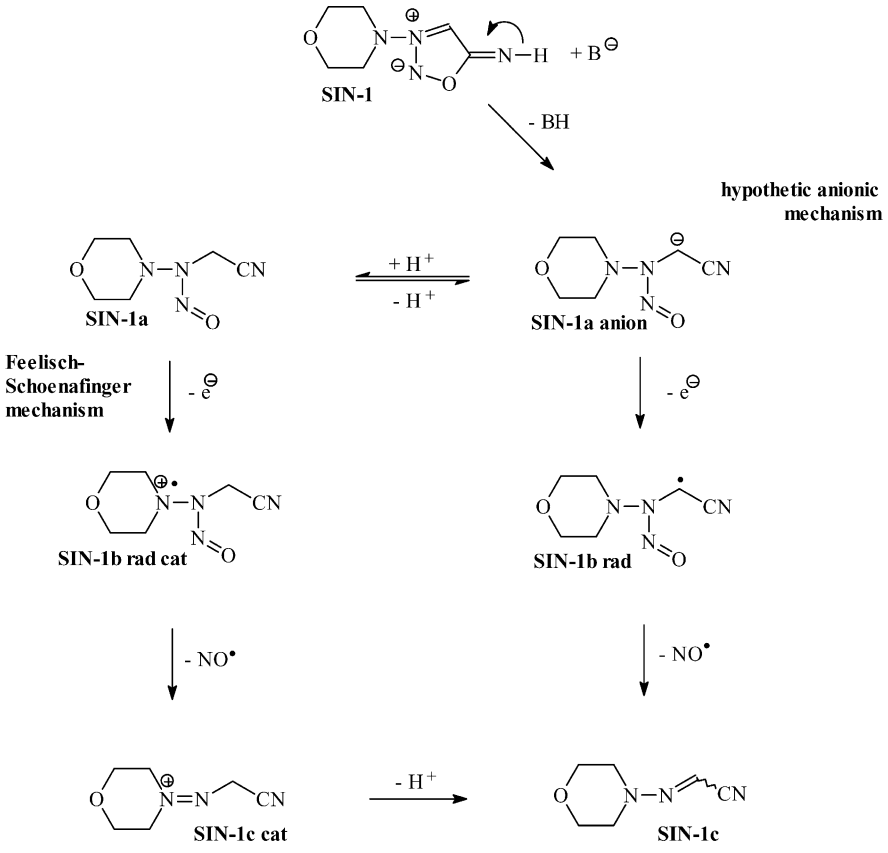

Scheme 1 Possible pathways of **SIN-1** decomposition: Feelisch–Schoenafinger mechanism and hypothetical anionic route

Møller–Plesset calculations. [20] Further validation for this level of theory comes from the calculated electron momentum distribution, obtained from the Kohn–Sham approximation, of the HOMO of gas phase glycine. When compared to the experimental distribution obtained from electron momentum spectroscopy (EMS), the pBP–DFT approach proves to be in excellent agreement to the experiment, outperforming expensive Hartree–Fock computations using basis sets as high as 6-311++G**, [21] and similar results have been found subsequently using other density functionals and with other molecules. [22] Also, for example, in a recent study of conformationally labile tetrahydropyran derivatives, the pBP method exhibited a very similar performance to the widely established B3LYP method for cyclic, [23] and similar to MP2 methods for acyclic systems. [24]

Even though there exists very recent published evidence for using pBP-DN* theory with negatively charged species, [25] the possible weakness of the chosen level of theory in our study could lie with the anions computed, since no diffuse functions are included in the basis sets employed, which could lead to less reliable energy descriptions. [26]

All equilibrium geometries were fully optimized with subsequent frequency calculation and exhibited no imaginary frequencies which could indicate saddle points or other non-equilibrium states, unless specifically mentioned. All single point calculations were performed subsequent to the DFT optimizations using HF (closed shell species) or UHF (open shell species) theory with a 6-311G** basis set. Conformational barriers were computed using the Linear Synchronous Transit (LST) method, [27] employing the two conformers in question as initial guesses and using weighing factors (wf) on a scale from zero (reactant-like) to one (product-like), followed by single point calculations at the individual geometry corresponding to each weighing factor. Van der Waals adducts were computed as described in the text. Transition structures were obtained using the NOSYM-TRY keyword with the geometries pre-optimized at the maximum of the corresponding IRC, which was determined with the Linear Synchronous Transit (LST) method followed by N2–N3 constrained optimization to provide the best initial guess possible (details see text). All transition structures exhibit one and only one imaginary frequency corresponding to the bond forming or breaking process regarding the reaction in question, as revealed by vibrational sequence analysis (VSA). All energies given in Figs. 1, 2, 3 and 4 are in hartrees, with opt=from DFT geometry optimization, and sp=from subsequent ab initio single point calculation. Frequencies were not scaled.

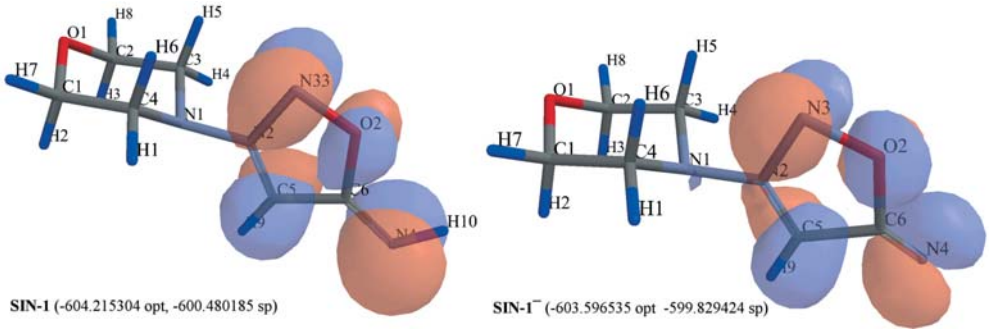

Fig. 1 DFT structures showing the HOMOs and DFT energies [htr] of **SIN-1** and the hypothetical anion **SIN-1**$^-$ (with O2–C6 bond constrained)

Results and discussions

SIN-1 and SIN-1$^-$

The lowest energy DFT structure of **SIN-1** is depicted in Fig. 1, and some selected parameters are shown in Table 1. This sydnonimine exhibits an N1–N2 bond length of 1.412 Å, suggesting a single bond between the morpholino- and the sydonimine moiety, which is plausible when comparing to the findings of Improta et al. for the corresponding sydnone derivatives. [13] Mulliken population analysis indicates no significant positive or negative charge for N2, a result that supports the fact that no significant π–π interaction between N1 and N2 exists, a consequence of the fact that morpholino- and sydnonimine moieties are positioned almost perpendicular to each other. Hence, the morpholino-nitrogen is largely sp^3 hybridized, as evidenced by the angle C4–N1–C3 of 110.84° and the fact that the HOMO is located in the sydnonimine part of the molecule exclusively. Deprotonation of **SIN-1** at N4 leads to the corresponding anion **SIN-1**$^-$, whose data are also displayed for comparison in Table 1 and Fig. 1. It is of theoretical interest only, since it exhibits two imaginary frequencies, unassociated with any bond breaking or forming, and is hence neither an equilibrium nor a transition state, and an imposed constraint at the O2–C6 bond was necessary for successful optimization.

SIN-1a and SIN-1a$^-$

Removing the constraint from **SIN-1**$^-$ and subsequent DFT optimization leads to ring opening of the sydnonimine and results in **SIN-1a**$^-$. The anionic charge is located in the sydnonimine part only, and that part of the structure is almost flat for orbital delocalization and perpendicular to the morpholine part. The conformer with the NO group turned towards the H5 and H6 of the morpholino moiety is slightly higher in energy at the DFT level[1]. **SIN-1a**$^-$ is therefore assumed to be the lowest energy conformer found in this study[2]. Mulliken population analysis of this conformer shows largest parts of the electron density on O2 (Table 2), supported by the electrostatic potential mapped on the 0.002 isodensity surface (Fig. 2), predicting that C5 protonation would most likely occur with assistance of the NO group. Indeed, when following the IRC, the so identified van der Waals adduct **SIN-1a**$^-$**H**$^+$**vdW** is essentially a hydroxylamine, as evidenced by the bond-electron density map shown in Fig. 2 (see also Table 2). It is relatively unstable since it involves significant charge separation between N2 and C5, as evidenced by the corresponding Mulliken charges and since the former sydnonimine part is twisted out of its preferred perpendicular position with respect to the morpholine moiety (Table 2, second row). The intrinsic barrier to eventually form the C5–H10 bond from **SIN-1a**$^-$**H**$^+$**vdW** is calculated to be only 1.62 kcal mol^{-1}, and the corresponding transition structure **SIN-1a**$^-$**H**$^+$**ts** is shown also in Fig. 2 and details are outlined in Table 2. Resulting from this approach is of course **SIN-1a** itself, which, with 2.149 Å distance, still

Table 1 Selected structural parameters and Mulliken charges of SIN-1 and SIN-1$^-$ (from DFT calculation)

	SIN-1	SIN-1$^-$
∠ Plane 1, N1, N2[a] [°]	6.36	6.64
∠ Plane 1, Plane 2[a] [°]	89.46	89.52
∠ C4, N1, C3 [°]	110.84	110.35
N1–N2 [Å]	1.412	1.441
N2–N3 [Å]	1.318	1.329
N3–O2 [Å]	1.395	1.444
O2–C6 [Å]	1.458	constrained at 1.458
C6–C5 [Å]	1.428	1.490
C5–N2 [Å]	1.344	1.327
C6–N4 [Å]	1.276	1.237
Mulliken N1 [au]	–0.27	–0.27
Mulliken N2 [au]	0.05	0.04
Mulliken N3 [au]	–0.01	–0.14
Mulliken O2 [au]	–0.31	–0.35
Mulliken C6 [au]	0.24	0.03
Mulliken C5 [au]	–0.06	–0.14
Mulliken N4 [au]	–0.43	–0.52
Imaginary frequency [cm^{-1}]	n.a.	164.91, 85.35

[a] Plane 1: C4,C3,C2 Plane 2: C5,N2,N3. Atom assignments see Fig. 1

[1] 28. –603.652651 opt, and –599.908077 sp, at DFT and ab initio level, respectively (structure not shown). Note that in contrast to the DFT level, the single point ab initio energy is slightly lower for this conformer compared to the one for **SIN-1a**$^-$.

[2] Another conformer with the N1–N2 bond turned 180° is slightly higher in energy and is therefore not considered.

Table 2 Structural features of SIN-1a, SIN-1a$^-$H$^+$ts, SIN-1a$^-$vdW and SIN-1a$^-$ (from DFT calculation)

	SIN-1a	SIN-1a$^-$H$^+$ts	SIN-1a$^-$H$^+$vdW	SIN-1a$^-$
∠ Plane 1, N1, N2[a] [°]	7.82	9.55	9.48	4.40
∠ Plane 1, Plane 2[a] [°]	87.51	43.29	50.80	89.49
∠ C4, N1, C3 [°]	111.19	112.31	111.61	111.45
N1–N2 [Å]	1.400	1.393	1.404	1.423
N2–N3 [Å]	1.355	1.312	1.306	1.337
N3–O2 [Å]	1.232	1.319	1.355	1.279
C6–C5 [Å]	1.461	1.424	1.412	1.393
C5–N2 [Å]	1.474	1.433	1.393	1.406
C6–N4 [Å]	1.168	1.176	1.177	1.191
H10–C5 [Å]	1.112	1.622	1.900	n.a.
H10···O2 [Å]	2.149	1.123	1.025	n.a.
Mulliken N1 [au]	–0.25	–0.21	–0.23	–0.27
Mulliken N2 [au]	–0.09	0.06	0.07	–0.02
Mulliken N3 [au]	0.14	0.08	0.03	–0.02
Mulliken O2 [au]	–0.31	–0.31	–0.30	–0.45
Mulliken C6 [au]	0.06	0.05	0.01	–0.01
Mulliken C5 [au]	–0.22	–0.45	–0.35	–0.25
Mulliken N4 [au]	–0.15	–0.19	–0.17	–0.33
Imaginary frequency [cm^{-1}]	n.a.	522.55	58.18	n.a.

[a] Plane 1: C4, C3, C2 Plane 2: C5, N2, N3. Atom assignments see Fig. 2

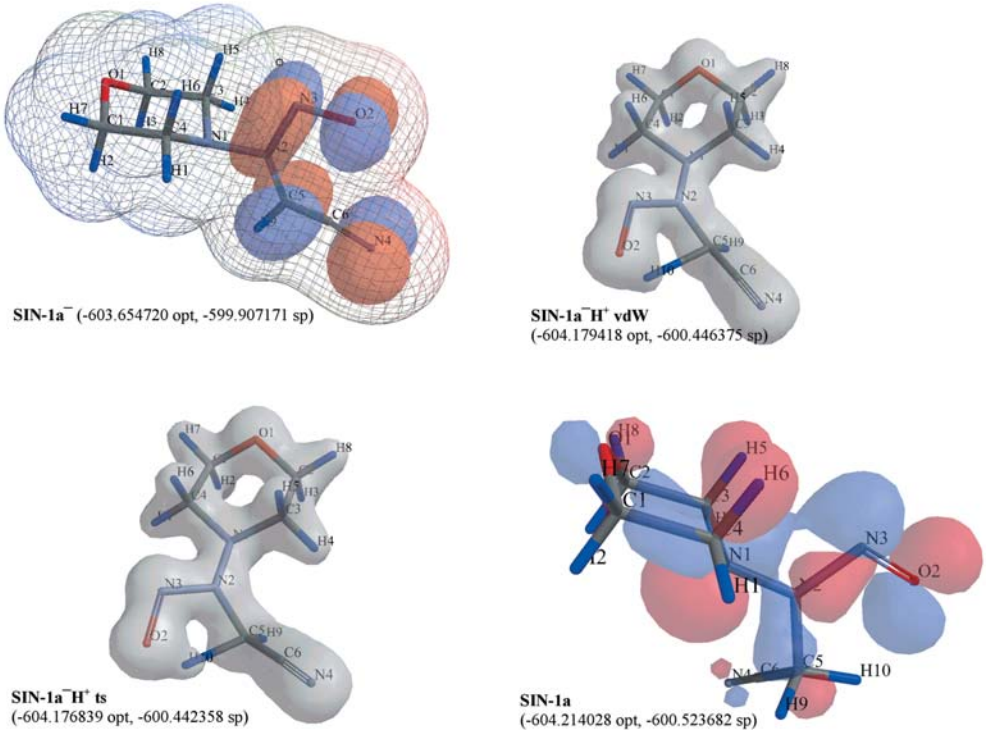

Fig. 2 Ring opened **SIN-1a$^-$** (from **SIN-1**$^-$ with constraint removed) with HOMO and electrostatic potential mapped on 0.002 isodensity surface (*red*=negative potential, *blue*=positive potential), the protonated van der Waals adduct and the corresponding transition structure with their 0.08 isodensity surfaces, and **SIN-1a** with HOMO after protonation of **SIN-1a$^-$** at C5

shows a notable possibility for H10···O2 through space stabilization.

When turning the NO group of **SIN-1a** towards the H5 and H6 hydrogens of the morpholino moiety, the resulting conformer arises with a slightly higher total energy[3]. Also, with reported NO turn-barriers of 21–25 kcal mol^{-1} for several N–NO compounds, [28] including *N*-nitrosopiperidines, which do allow enantiomeric resolution by inclusion crystallization using optically active diols, they are likely too large to render any other NO-turned conformer of **SIN-1a$^-$** or **SIN-1a** highly populated. Therefore **SIN-1a** is used for all further studies of the Feelisch–Schoenafinger pathway.

The more complex question of whether **SIN-1a** or **SIN-1a$^-$** is the prevalent species in **SIN-1** activation is more difficult to address, especially when comparing to equilibrium situations in solution, mainly because there is no direct correlation between kinetic acidity and thermodynamic acidity of C–H acidic compounds. [29] Since this work is aimed at intrinsic reactivities only, both pathways will be considered and discussed.

[3] –604.211827 opt, –600.522470 sp, structure not shown.

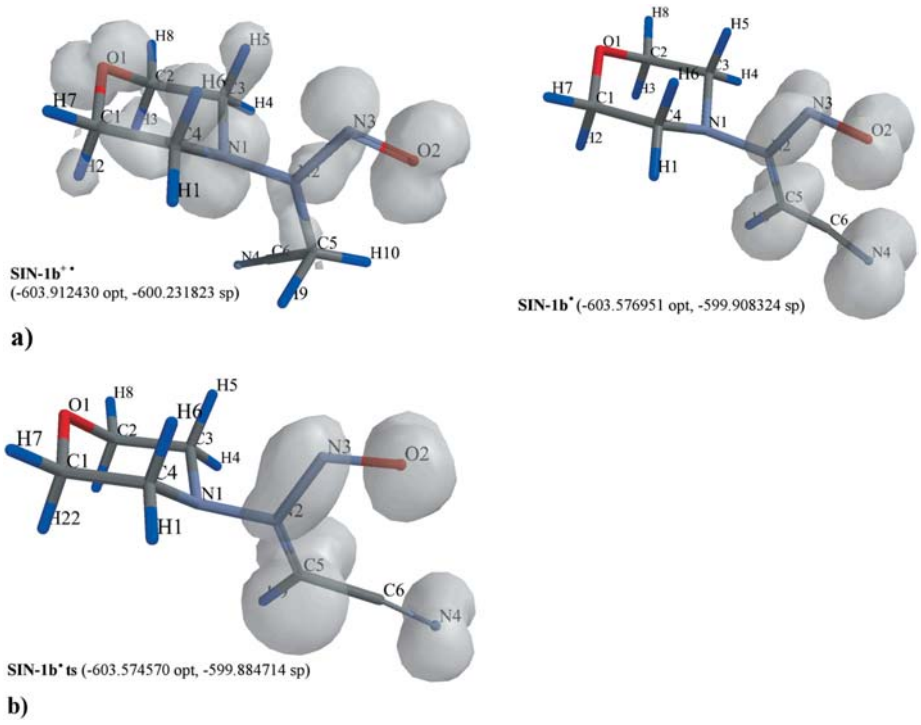

Fig. 3 a DFT structures showing spin density distributions of **SIN-1b**$^{\cdot+}$ (derived from **SIN-1a**) and **SIN-1b**$^{\cdot}$ (derived from **SIN-1a**$^{-}$). **b** DFT transition structure of the radical **SIN-1b**$^{\cdot}$ showing spin density distribution

Table 3 Selected structural features of SIN-1b$^{\cdot+}$ and of SIN-1b$^{\cdot}$ and the transition structure SIN-1b$^{\cdot}$ ts (from DFT calculation)

	SIN-1b$^{\cdot+}$	SIN-1b$^{\cdot}$	SIN-1b$^{\cdot}$ ts
∠ Plane 1, N1,N2[a] [°]	36.44	7.51	4.55
∠ Plane 1, Plane 2[a] [°]	85.63	89.86	77.09
∠ C4, N1, C3 [°]	117.89	110.82	111.07
N1–N2 [Å]	1.348	1.409	1.398
N2–N3 [Å]	1.448	1.431	1.679
N3–O2 [Å]	1.189	1.228	1.191
C6–C5 [Å]	1.461	1.399	1.409
C5–N2 [Å]	1.485	1.359	1.337
C6–N4 [Å]	1.167	1.181	1.179
H9–C5 [Å]	1.110	n.d.	n.d.
H10–C5 [Å]	1.112	n.d.	n.d.
H10···O2 [Å]	2.192	n.a.	n.a.
H4···H9 [Å]	n.d.	n.d.	n.d.
Mulliken N1 [au]	–0.13	–0.28	–0.26
Mulliken N2 [au]	–0.13	–0.04	–0.11
Mulliken N3 [au]	0.22	0.10	0.08
Mulliken O2 [au]	–0.11	–0.25	–0.15
Mulliken C6 [au]	0.06	0.03	0.01
Mulliken C5 [au]	–0.27	–0.04	–0.03
Mulliken N4 [au]	–0.10	–0.15	–0.15
Imaginary frequency [cm^{-1}]	n.a.	n.a.	171.07
$\langle S^2 \rangle$[b]	0.751	0.753	0.753

[b] Plane 1: C4, C3, C2 Plane 2: C5, N2, N3. Atom assignments see Fig. 3.
[b] Total spin. Ideal value for doublet open shell systems: 0.750 from $s(s+1)$ with s=1/2.

SIN-1b$^{\cdot+}$ and SIN-1b$^{\cdot}$

Removing one electron from **SIN-1a** and **SIN-1a**$^{-}$ and subsequent DFT geometry optimization results in the formation of radical cation **SIN-1b**$^{\cdot+}$ and the neutral radical **SIN-1b**$^{\cdot}$, respectively, as depicted in Fig. 3a and described in Table 3.

The radical cationic pathway is most interesting, but also the most complex. This is mainly because removal of the electron results in weakening of the stabilizing H10···O2 interaction going from a distance of 2.149 Å (**SIN-1a**) to 2.192 Å (**SIN-1b**$^{\cdot+}$), and further step-by-step elongation of the N2–N3 bond, following the IRC path for NO loss, apparently results in conformational lability of the position of the CH_2–CN group. All corresponding geometry as well as transition state optimizations converged easily but yielded one to two imaginary frequencies at around 30–60 cm^{-1}, all of which represent torsional movements of the CH_2–CN group around the N2–C5 bond, plus a sidewise movement around the N1–N2 bond, but no apparent displacement of the NO group. This is visualized in Scheme 2, along with the corresponding IRC. The latter can only be a guess, since in this case at this level of theory, any attempt, including the freezing of atoms, to eliminate the imaginary frequencies was unsuccessful, and a clean transition structure could not be obtained. While there is precedent in the literature for possible artifacts of DFT theory when dealing with open shell species, [30] it is also likely that a too flat potential energy surface is the reason why no proper transition state for NO loss could be found within the scope of this work.

The thermodynamics of the Feelisch–Schoenafinger pathway compute as follows: one-electron oxidation of **SIN-1a** to **SIN-1b**$^{\cdot+}$ requires 183.14 kcal mol^{-1}, which translates to 7.94 eV. Then, further activation through NO loss is best guessed to require about 0.9 kcal mol^{-1}, indicated in Scheme 2. It should be mentioned that this

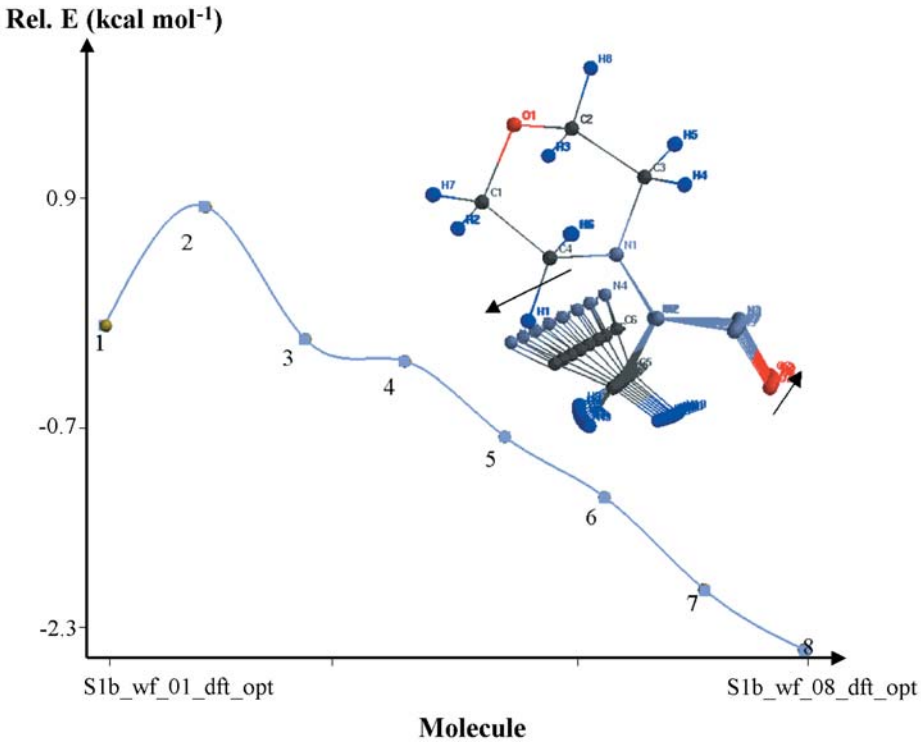

Scheme 2 Torsional movements and IRC estimate in the radical-cationic Feelisch–Schoenafinger mechanism as a function of N2–N3 bond elongation (NO displacement). N2–N3 distances: 1=1.4484; 2=1.4486; 3=1.4489; 4=1.4493; 5=1.4497; 6=1.4502; 7=1.4507; 8=1.4512

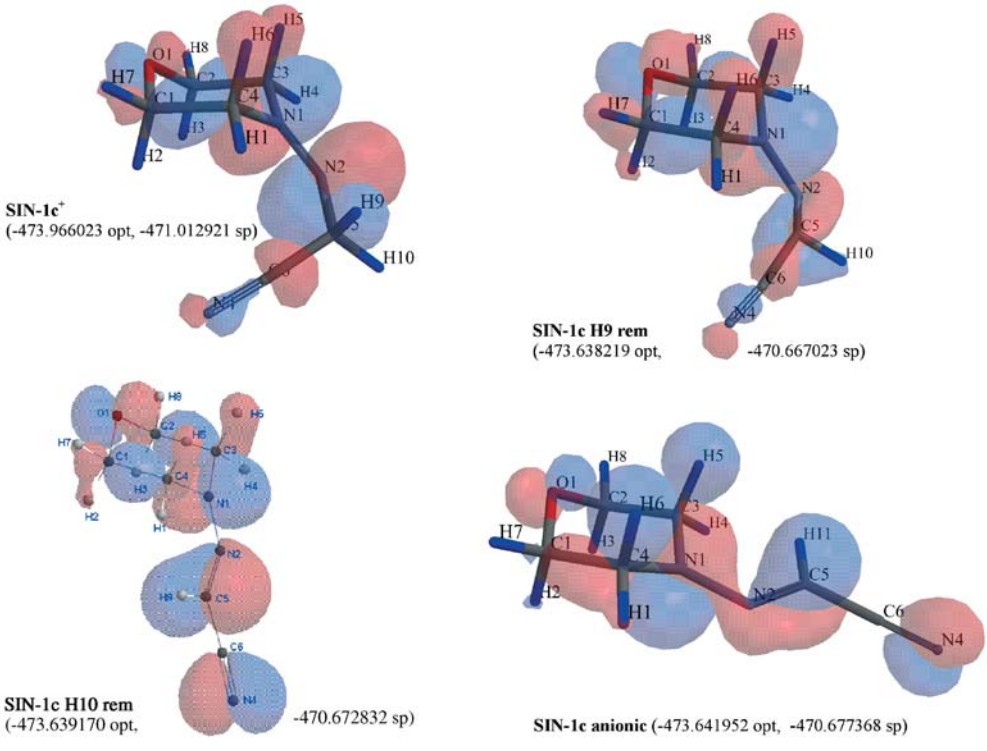

Fig. 4 Structures of **SIN1c**$^{+}$, the H9 removed and H10 removed **SIN-1c** conformers, all from the Feelisch–Schoenafinger pathway, as well as the resulting **SIN-1c** conformer from the anionic pathway. The cation shows the LUMO, all others show the HOMOs

"guess" might be entirely due to the CH_2–CN lability rather than having any true intrinsic reaction barrier component.

In contrast, the anionic pathway appears to be less elusive. One-electron removal from **SIN-1a**$^{-}$ and geometry optimization results in **SIN-1b**$^{\cdot}$ as displayed in Fig. 3 and described in Table 3. Following the IRC, the transition structure **SIN-1b**$^{\cdot}$ **ts** with exactly one imaginary frequency at 171.07 cm^{-1} (Table 3, Fig. 3b), showing a displacement along the N2–N3 bond vector. For this pathway, two steps

Table 4 Structural features of SIN-1c$^+$ and SIN-1c (from DFT calculation)

	SIN-1c$^+$	SIN-1c H10 rem	SIN-1c H9 rem	SIN-1c anionic
∠ Plane 1, N1, N2[a] [°]	57.48	78.82	62.31	16.65
∠C4, N1, C3 [°]	113.50	112.19	112.60	115.22
N1–N2 [Å]	1.257	1.330	1.317	1.330
N2–C5 [Å]	1.482	1.308	1.314	1.308
C5–H9 [Å]	1.114	1.105	n.a.	n.a.
C5–H10 [Å]	1.106	n.a.	1.099	1.105
H4···H9 [Å]	n.d.	n.a.	n.a.	2.029
H1···H9 [Å]	2.179	1.985	n.a.	n.d.
Mulliken N1 [au]	–0.01	–0.18	–0.18	–0.17
Mulliken N2 [au]	–0.04	–0.07	–0.07	–0.06
Mulliken C6 [au]	0.05	0.04	–0.04	0.04
Mulliken C5 [au]	–0.31	–0.15	–0.15	–0.15
Mulliken N4 [au]	–0.09	–0.17	–0.18	–0.17
Imaginary frequency [cm^{-1}]	n.a.	n.a.	63.45	n.a.

[a] Plane 1: C4, C3, C2. Atom assignments see Fig. 4

apply. First, the oxidation potential of **SIN-1a**$^-$ yielding **SIN-1b**$^\cdot$ computes to –0.72 kcal mol^{-1}; hence that step would be intrinsically exothermic. Second, to promote NO loss from **SIN-1b**$^\cdot$, 14.82 kcal mol^{-1} are calculated to be necessary, suggesting an overall intrinsic barrier of only 14.09 kcal mol^{-1}.

Not unexpectedly, both spin density distributions of the radical cationic structure **SIN-1b**$^{\cdot+}$ and the neutral radical structure **SIN-1b**$^\cdot$ look very different and reflect the distribution of the HOMOs of their respective predecessors, **SIN-1a** and **SIN-1a**$^-$. In contrast to the anionic route, in the cationic pathway, large parts of the morpholino moiety are predicted by DFT theory to participate in the density distribution. There is precedence for this pattern as reported in the case of *N*-alkylnitrosamines. [31]

SIN-1c$^+$ and SIN-1c

Removal of the NO group from both, the cationic **SIN-1b**$^{\cdot+}$**vdW** and the neutral and **SIN-1b**$^\cdot$**vdW**, and subsequent DFT optimization results in **SIN-1c**$^+$ and **SIN-1c**, respectively, which are shown in Fig. 4 and described in Table 4.

Removing H9 and H10 from the corresponding deprotonation–van der Waals adducts (not shown) of **SIN-1c**$^+$, leads to **SIN-1c H9rem** and **SIN-1c H10rem**, respectively. The former is *Z*-configured, while the latter assumes the energetically favored *E*-configuration at the N2–C5 double bond. Conversion of the latter to the lowest energy conformer, **SIN-1c anionic**, obtained directly from NO loss of **SIN-1b**$^\cdot$ **vdW**, computes to a quite significant 11.927 kcal mol^{-1}. Typical experimental values for N–N rotations range from 14 to around 20 kcal mol^{-1}. [32] Consequently, and in contrast to **SIN-1** above, slightly widened angles C4–N1–C3 of around 112–115° as well as shorter bond distances of around 1.32–1.33 Å do suggest some double bond character between N1 and N2 for the **SIN-1c** structures.

Summary and conclusions

In a first effort to fill the striking gap of physico-chemical data in the area, two possible intrinsic reaction pathways of **SIN-1** decomposition have been explored using DFT theory. The most notable results thus predicted are: **SIN-1a** is lowest energy species, but total activation along the Feelisch–Schoenafinger pathway would take about 183.14+0.9 kcal mol^{-1}=184.04 kcal mol^{-1} or 7.94+ 0.04 eV=7.98 eV. In contrast, the one-electron removal from the anionic **SIN-1a**$^-$ is predicted to be slightly exothermic with the overall activation energy computing to 14.09 kcal mol^{-1} or 0.61 eV. These findings are summarized in Scheme 3. Some of the data provided in this work, especially the thermodynamic feasibility of the anionic pathway, might be of interest to future bioavailability studies, for example in environments where proton availability might be scarce, i.e. in lipid membranes, myelinic structures of neurons or the blood brain barrier. [9] Future work should include excited states, condensed phase modeling and higher levels of theory for the cationic pathway in order to address issues such as NO$^\cdot$ versus NO$^+$ emission. With respect to the well known drug applications of **SIN-1** in the form of molsidomine, important barrier crossings such as the gut, i.e. Caco-2 cell models, [33] or the blood–brain barrier partitioning coefficients [34] could be studied computationally.

Equipment and software

All calculations were carried out on a Silicon Graphics Power Indigo 2XZ workstation with an R8000 175-MHz processor, and a Silicon Graphics 4xR4400 150-MHz Challenge server with SGI IRIX 64 Release 6.5 mounted, using the SPARTAN molecular modeling software package V5. [35] All graphical molecule depictions but the one in Scheme 2 were created in Spartan '04 for Windows. [36]

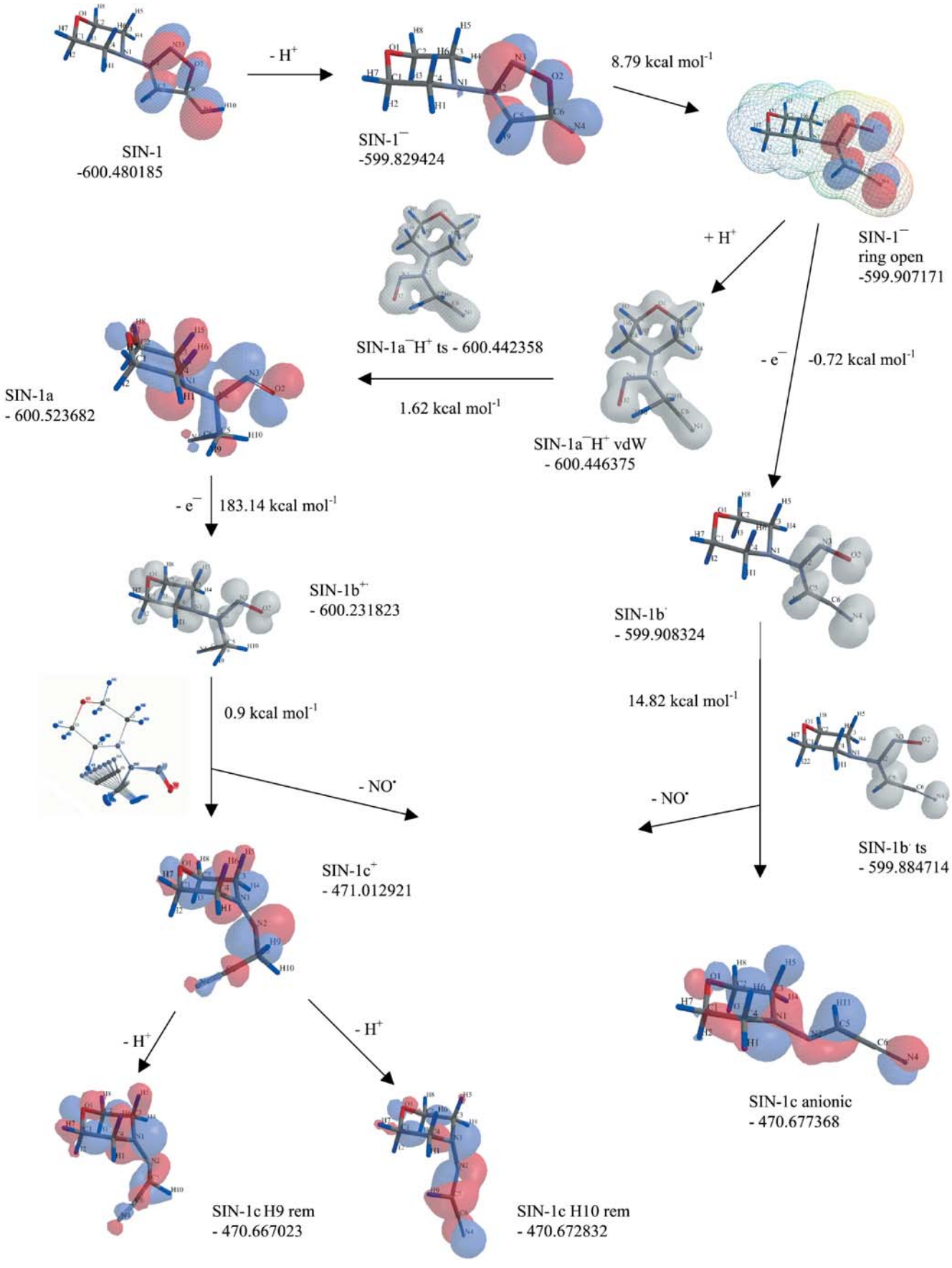

Scheme 3 Summary of pathways and highlights of energetic findings. Unless otherwise mentioned, energies are in hartrees from single point calculations

Acknowledgements The author gratefully acknowledges the kind support of Drs. Karl F. Moschner and Stephen A. Madison as well as Mr. Anthony G. Cece, all Unilever Research US, and is grateful for their permission to utilize the above mentioned workstations. The author also thanks the referees for a helpful comment.

References

1. (a) Gilchrist TL, O'Neill PM (1996) In: Katritzky AR, Pozharskii AF (eds) Comprehensive heterocyclic chemistry II, vol 4. Pergamon, Oxford, pp 168–175; (b) Ramsden CA (1979) In: Barton DHR, Ollis WD (eds) Comprehensive organic chemistry, vol 4. Pergamon, Oxford, pp 1171–1228; (c) Yashunskii VG, Kholodov LE (1980) Russ Chem Rev 49:54–91; (d) Sugimoto J, Syoji N, Mizuno K, Morita M (1984) Jpn Circ J 48:1091–1096; (e) Ackermann E (1967) Pharmazie 22:537–542; (f) Rosenkranz B, Winkelmann BR, Parnham MJ (1996) Clin Pharmacokinet 30:372–384;(g) Reden J (1990) Blood Vessels 27:282–294; (h) Madison SA, McCallum JEB, Rojas Wahl RU (1999) US 5914305, WO 99/21950, EP1027416, AN 130:326574 CA
2. Rojas Wahl RU, Madison SA, McCallum JEB (2000) Tens Surfact Deterg 37:83–89
3. (a) Palmer MJ, Ferrige AG, Moncada S (1987) Nature 327:524–526; (b) Dimmeler S, Zeiher AM (2000) In: Loscalzo L, Vita JA (eds) Nitric oxide and the cardiovascular system. Humana, Totowa, pp 69–84
4. Ishikawa Y, Iida H, Ishida H (2002) Mol Pharmacol 61:1423–1434
5. Chopp M, Zhang R (2002) Caym Currents 11:5
6. (a) Arnett H, Hellendall RP, Matsushima GK, Suzuki K, Laubach VE, Sherman P, Ting JPY (2002) J Immunol 168:427–433; (b) Bizzozero OA, Bixler H, Parkhani J, Pastuszyn A (2001) Neurochem Res 26:1127–1137; (c) Smith KJ, Kapoor R, Hall SM, Davies M (2001) Ann Neurol 49:470–476; (d) van der Veen RC, Roberts LJ (1999) J Neuroimmunol 95:1–7; (e) Smith KJ, Kapoor R, Felts PA (1999) Brain Pathol 9:69–92; (f) Atkins CM, Sweatt JD (1999) J Neurosci 19:7241–7248
7. (a) Fatemi SH, Cuadra AE, El-Fakahany EE, Sidwell RW, Thuras P (2000) Neuroreport 11:1493–1496; (b) Lombard J (1998) Med Hypothesis 50:497–500; (c) Sogut S, Zoroglu SS, Ozyurt H, Ramazan Yilmaz H, Ozurgurlu F, Sivasli E, Yetkin O, Yanik M, Tutkun H, Savas HA, Tarakcioglu M, Akyol O (2003) Clin Chim Acta 331:111–117
8. Stern J, Ludwig M (2001) Am J Physiol Regulat Integrat Comp Physiol 280:R1815-R1822
9. Mayhan WG (2000) Brain Res 866:101–108
10. (a) Feelisch M, Noack E (1987) Eur J Pharmacol 139:19–30; (b) Feelisch M, Noack E (1987) Eur J Pharmacol 142:465–469; (c) Feelisch M, Ostrowski J, Noack E (1989) J Cardiosvasc Pharm 14:S13-S22; (d) Feelisch M (1991) J Cardiovasc Pharm 17:S25-S33; (e) Bohn H, Schoenafinger K (1989) J Cardiovasc Pharm 14:S6-S12; (f) Schoenafinger K (1999) Farmaco 54:316–320
11. Singh RJ, Hogg N, Joseph J, Konorev E, Kalyanaraman B (1999) Arch Biochem Biophys 361:331–339
12. (a) Petride H, Cort AD, Florea C, Caproiu M (1999) Rev Roumaine Chimie 44:249–259; (b) Giordano F (1988) Gazz Chim Ital 118:501–505
13. Improta R, Santoro F, Barbier C, Giordano F, del Re G (1998) J Mol Struct (THEOCHEM) 433:291–299
14. Pitsikas N, Rigamonti AE, Cella SG, Muller EE (2002) Psychopharmacology 162:239–245
15. Ullrich T, Oberle S, Abate A, Schroder H (1997) FEBS Lett 406:66–68
16. Vikmon M, Szente L, Geczy JM, Bult H, Malinski T, Feelisch M (1996) Portland Press Proc 10:188
17. Becke AD (1988) Phys Rev A 38:3098–3100
18. Perdew JP (1986) Phys Rev B 33:8822–8824
19. Hehre WJ, Lou L (1997) A guide to density functional calculations in Spartan. Wavefunction Inc, Irvine, Calif.
20. Lewars E (2000) Can J Chem 78:297–306
21. Zheng Y, Neville JJ, Brion CE (1995) Science 270:786–788
22. (a) Rolke J, Zheng Y, Brion CE, Shi Z, Wolfe S, Davidson ER (1999) Chem Phys 244:1–24; (b) Litvinyuk IV, Young JB, Zheng Y, Cooper G, Brion CE (2001) Chem Phys 263:195–201; (c) Litvinyuk IV, Zheng Y, Brion CE (2000) Chem Phys 261:289–300
23. Freeman F, Kasner ML, Hehre WJ (2001) J Phys Chem A 105:10123–10132
24. Hehre WJ, Yu Y, Klunzinger PE, Lou L (1998) A brief guide to molecular mechanics and quantum chemical calculations. Wavefunction Inc, Irvine, Calif.
25. Hesske H, Gloe K, Goretzki G, Grotjahn M, Langer M, Wichman K, Gloe K, Nouaman M, Yoshizuka K (2003) Anion and cation binding of aminopodands: complexation and molecular modeling studies. In: 17th Darmstaedter Molecular Modelling Workshop, Computer Chemistry Center, University Erlangen-Nuernberg, p. 18
26. Hehre WJ (2003) A guide to molecular mechanics and quantum chemical calculations. Wavefunction Inc, Irvine, Calif., pp 166–168
27. Halgren TA, Lipscomb WN (1977) Chem Phys Lett 49:225–232
28. (a) Olszewska T, Milewska MJ, Gdaniec M, Maluszynska H, Polonski T (2001) J Org Chem 66:501–506; (b) Cooney JD, Brownstein SK, ApSimon JW (1974) Can J Chem 52:3028–3036; (c) Fraser RR, Ng LK (1975) J Am Chem Soc 98:5895–5899
29. Sykes P (1988) Reaktionsmechanismen der Organischen Chemie—Eine Einfűhrung, 9th edn. VCH, Weinheim, pp 329–330
30. Deng QL, Thomas BE, Houk KN, Dowd P (1997) J Am Chem Soc 119:6902–6908
31. Jiang P, Qian X, Li C, Qiao C, Wang D (1997) Chem Phys Lett 277:508–512
32. Green DVS, Hillier IH, Morris GA, Gensmantel N, Payling DW, Robinson DH (1991) J Mol Struct (THEOCHEM) 251:173–193 and references therein
33. Kulkarni A, Han Y, Hopfinger AJ (2002) J Chem Inf Comput Sci 42:331–342
34. Rose K, Lowell HH (2002) J Chem Inf Comput Sci 42:651–666
35. Spartan Version 5 (1997) Wavefunction Inc, 18401 Von Karman Avenue, Suite 370, Irvine, CA 92612, USA
36. Spartan '04 (2003) Wavefunction Inc, Irvine, CA